frontiers | Frontiers in Energy Research

TYPE Original Research
PUBLISHED 29 November 2024
DOI 10.3389/fenrg.2024.1441746

OPEN ACCESS

EDITED BY
Samuel Simon Araya,
Luxembourg Institute of Science and Technology (LIST), Luxembourg

REVIEWED BY
Xin Gao,
Technical University of Braunschweig, Germany
Xi Lin,
Shanghai Jiao Tong University, China

*CORRESPONDENCE
Michél Hauer,
michel.hauer@igp.fraunhofer.de

RECEIVED 31 May 2024
ACCEPTED 14 November 2024
PUBLISHED 29 November 2024

CITATION
Hauer M, Schmidt S, Gericke A, Brätz O, Möhrke L, Biswal P, Stroetmann N and Henkel K-M (2024) A novel design approach: increase in storage and transport efficiency for liquid hydrogen by using a dual concept involving a steel-fiber composite tank and thermal sprayed insulating coatings. *Front. Energy Res.* 12:1441746. doi: 10.3389/fenrg.2024.1441746

A novel design approach: increase in storage and transport efficiency for liquid hydrogen by using a dual concept involving a steel-fiber composite tank and thermal sprayed insulating coatings

Michél Hauer[1]*, Stefan Schmidt[2], Andreas Gericke[3], Oliver Brätz[4], Lukas Möhrke[1], Pratidhwani Biswal[1], Nicco Stroetmann[1] and Knuth-Michael Henkel[5]

[1]Department Manufacturing Technologies, Thermal Coating Systems, Fraunhofer Institute for Large Structures in Production Engineering IGP, Rostock, Germany, [2]Department New Processes and Materials, Fiber Composite Technologies, Fraunhofer Institute for Large Structures in Production Engineering IGP, Rostock, Germany, [3]Department Manufacturing Technologies, Department Lead, Fraunhofer Institute for Large Structures in Production Engineering IGP, Rostock, Germany, [4]Department Manufacturing Technologies, Thermal Joining Engineering, Fraunhofer Institute for Large Structures in Production Engineering IGP, Rostock, Germany, [5]Faculty of Mechanical Engineering and Marine Technologies, Chair of Joining Technology, University of Rostock, Rostock, Germany

Wind power-to-gas concepts have a high potential to sustainably cover the increasing demand for hydrogen as an energy carrier and raw material, as it has been shown in the past that there is an enormous potential in energy overproduction, which currently remains unused due to the shutdown of wind turbines. Thus, there is barely experience in maritime production, offshore storage, and transport of large quantities of liquid hydrogen (LH_2) due to the developing market. Instead, tank designs refer to heavy standard onshore storage and transport applications with vacuum insulated double wall hulls made from austenitic stainless steel and comparatively high thermal diffusivity and conductivity. This reduces cost effectiveness due to inevitable boil-off and disregards some other requirements such as mechanical and cyclic strength and high corrosion resistance. Hence, new concepts for LH_2 tanks are required for addressing these issues. Two innovative technical concepts from space travel and high-temperature applications were adopted, combined and qualified for use in the wind-power-to-gas scenario. The focus was particularly on the high requirements for transport weight, insulation and cryogenic durability. The first concept part consisted of the implementation of FRP (fiber-reinforced plastics)–steel hybrid tanks which have a high potential as a hull for LH_2 tanks. However, these hybrid tanks are currently only used in the space sector. Questions still arise regarding interactions with coatings, production, material, temperature resilience and design for commercial use. Thermally sprayed thermal barrier coatings (TBC) in turn show promising potential for surfaces subject to high thermal and

mechanical stress. However, the application is currently limited to use at high temperatures and needed to be extended to the cryogenic temperature range. The research on this second part of the concept thus focused on the validation of standard MCrAlY alloys and innovative (partially) amorphous metal coatings with regard to mechanical-technological and insulating properties in the low temperature range. This article gives an overview regarding the achieved results including manufacturing and measurements on a small tank demonstrator.

KEYWORDS

liquid hydrogen, thermal spray, thermal barrier coating, cryogenic testing, insulation, filament winding

1 Introduction

In the context of the energy transition and steadily rising energy demand, the production of hydrogen from renewable energy sources is increasingly becoming the focus of public attention in business and politics. The German government's hydrogen strategy (German, 2020) and the European Commission's Green Deal (European Commission, 2020) underline the vehemence of these developments. The focus is not only on the possibility of storing green energy and ensuring national energy security that is as autonomous as possible, but also on a promising market for the production and sale of green hydrogen. In addition to traditional hydrogen processing for ammonia synthesis, for example, industrial demand as a raw material will increase significantly. This includes fuel cell-based mobility solutions and, for example, direct reduction in steel production using hydrogen (DRI, direct reduced iron). DRI has already been established as an indispensable technology for achieving climate objectives and is forecast to require 6 TWh of hydrogen per year (Fraunhofer and Fraunhofer, 2024). Currently, hydrogen is used almost exclusively as a chemical raw material and not as an energy storage medium. Many international activities show that this will change in the future. In particular, wind power-to-gas concepts have a high potential to sustainably cover the increasing demand for hydrogen as an energy source and raw material. It has been shown in the past that there is enormous energy potential in energy overproduction, which currently remains unused by shutting off offshore wind turbines (Fraunhofer and Fraunhofer, 2024; FrostSullivan, 2020). Thus, there is currently no experience with maritime generation, storage, and transportation of large quantities of LH_2 due to the developing market. However, it is clear that certain requirements must be fulfilled, particularly for maritime transportation. In addition to corrosion, this applies in particular to static and/or fatigue strength in the event of hydrodynamic wave formation (sloshing), impact as well as a reduction of transport weight. Low dynamic amplitudes can lead to high sloshing forces, which may result in local plasticization and wear in small LH_2 tanks (cylindrical tank; diameter d = 3.5 m; height h = 2 m) (Liu et al., 2019). Furthermore, mechanical impact stresses can lead to phase transformations (γ to α) in the austenitic materials currently used with accompanying loss of ductility and cracking (Pinto et al., 2005).

In order to meet these demanding requirements, the focus initially shifted to special FRP steel hybrid tank concepts, which guarantee high mass-specific strength as well as increased protection against corrosion and are well established in the aerospace industry (Degenhardt, 2016). During the work, questions regarding interactions with coatings, production, material, temperature resistance and design for commercial use were investigated. A further requirement is the need to increase the insulation effect regarding boil-off losses in present double-walled and vacuum-insulated tanks. This boil-off is approx. 2% of the volume of stored liquid per day. During longer storage and transportation times, e.g., for several days, this leads to large losses and inefficiency (FrostSullivan, 2020). To counteract boil-off, the tank pressure can be adjusted, but the insulation effect must still be increased for sensible use (FrostSullivan, 2020). For this, TBC fabricated by thermal spraying processes have come into focus due to their high insulating effect and wear resistance to potentially reduce boil-off and additionally protect the tank shell from dynamic sloshing forces. Applications for TBC include, e.g., heavily loaded turbine and compressor blades or combustion chamber parts (Bach et al., 2005; Mathesius and Krömmer, 2014; Lima et al., 2017; Lima et al., 2019; Pawłowski, 2008; Terberger, 2015) and various turbine designs (Holloman and Levy, 1992; Vassen et al., 2009) for protection against hot gas and high-temperature corrosion. However, the use of this technology and materials is currently limited to high temperatures and was extended to the cryogenic temperature range by the several studies. The investigations focused on the validation of standard MCrAlY alloys and innovative (partially) amorphous iron-based coatings regarding mechanical-technological and insulating properties in low temperature under variation of different spraying processes and parameters such as porosity. Both, cost-effective conventional thermal spray technologies (Twin Wire Arc Spray, Atmospheric Plasma Spray) and somewhat more cost-intensive high-speed processes with high coating quality (High Velocity Oxygen Fuel Spray) were used for this purpose. The main factor influencing these technologies shall be briefly summarized in the following.

First, high velocity oxygen fuel spraying (HVOF) is characterized by short exposure times of the particles to the atmosphere. This results in only slight oxidation. Moreover, high impact velocities result in dense coating structures (Kreye et al., 2000; Wielage et al., 2006). It is a good possibility to gain superior coating properties while being well established on the market at the same time. When gas is used as fuel, the oxygen to fuel ratio can be manipulated into the sub-stoichiometric range (Krömmer et al., 2009; Dobler et al., 2000) or into the super-stoichiometric conditions, e.g., if higher porosity contents are desired. Spray systems using gas cooling of the combustion chamber wall as well as powder injection into the combustion chamber allow for a targeted manipulation of the oxidation of the spray material. A typical example of this is the gun Diamond Jet 2,700 (DJ2700) which is therefore used in the context of this work, see Figure 1A. Second, Arc Spray is a simple and cost-effective thermal spray technology, which is determined by

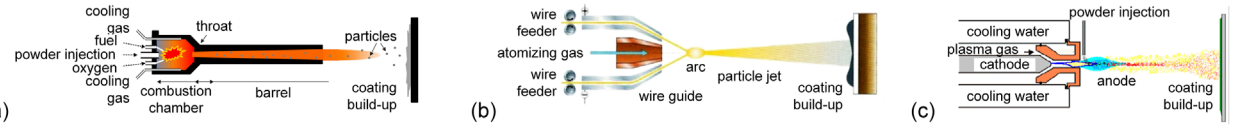

FIGURE 1
Scheme of the used thermal spray processes. *HVOF Spray* **(A)**, *Arc Spray* **(B)** and *Plasma Spray* **(C)**.

some key factors (Lang et al., 2015; Kim and Lee, 2010). Arc voltage and current of the wires and gas flow (e.g., free, forced, etc.), pressure, and type can affect coating quality (Lang et al., 2015; Chi et al., 2014) see also Figure 1B. Besides, residual stresses in the coatings are influenced by the parameters and spray kinematics like the stand-off distance, spray pattern, robot speed, etc. (Chi et al., 2014; Hauer et al., 2017). Since arc spraying is established, e.g., for corrosion protection of large structures, the technology was also considered for preparing metallic TBC on large components like inner tank hulls or pipelines for LH_2. Finally, in plasma spraying, a high-voltage pulse is used to ignite an arc that burns between a cathode (usually W) and a Cu anode nozzle, see Figure 1C. A gas (e.g., Ar, He, N_2, H_2) or gas mixture is fed into the nozzle via a gas distribution ring ionized by the arc and thus converted into plasma state. Temperatures of up to 20,000 K can occur in the resulting plasma jet, to which the spray material is fed using powder injectors. The process is therefore ideal for coating refractory materials such as conventional TBC systems consisting of a metallic bond coat (BC) with a ceramic top coat (TC) such as yttrium-stabilized zirconium oxide (YSZ) (Bach et al., 2005; Pawłowski, 2008).

This article gives an overview of selected achieved results regarding the dual concept including the fabrication and testing of a hybrid pipe as well as small hybrid tank demonstrator combining both, the fiber windings with the thermal spray coating. As tank designs vary to a huge degree, several tank building companies involved as consultants suggested these demonstrator types. Currently, isolating materials such as PU foams are used in LH_2 tanks, i.e., between the tank hulls. Yet, the boil-off still occurs due to regasification of the stored liquid medium. It therefore makes sense to improve the insulation in contact with, i.e., on the inside of the inner tank. As a first step, the developed two concepts and further promising results of the coatings such as high mechanical properties were thus to be combined on the outside of the inner hull to prove the general feasibility. The final results may lay the foundation for the future use of the dual concept not only in tanks but also in pipelines.

2 Materials and methods

The following four sections are a brief description of some of the key test methods. In the first part of this section, part of the initial work carried out on thermal spray coatings will be described.

Afterwards the methods and procedures regarding the technology demonstrator, i.e., pipe and tank demonstrator are presented in detail, including the fiber winding production.

2.1 Thermal spray experiments and base materials

The twin wire arc spraying tests (hereafter *Arc Spray*) were carried out with a DURUM Durspray 450 power source equipped with an ASJO2nd torch (T-Spray GmbH, Lenningen, DE). Details on parameters and material used can be found in Table 1. The experiments on HVOF (hereafter *HVOF Spray*) were carried out with a DJ 2700 torch (Oerlikon Metco Europe GmbH, Kelsterbach, DE). Parameters and the material used can be found in Table 2. Since TBC systems with a ceramic top layer show the best thermal insulation in the high-temperature range, comparative spray experiments were carried out with this system consisting of a NiCrAlY bond coat and YSZ ceramic. As the state of the art and the solution of choice for high-temperature applications, the metallic coatings had thus to be compared to the new coating systems. For this purpose, certain target characteristics, as described in the following sections, as well as process parameters had to be achieved. These are, for example, deposition efficiencies, achievable coating thicknesses, but also general processability with the particular spray technology. For this purpose, atmospheric plasma spraying (hereafter *Plasma Spray*) was used with a Delta PPC power source and a Delta RE torch (both GTV Verschleißschutz GmbH, Luckenbach, DE). The parameters and materials for this test series can be found in Table 3.

For assessing the suitability for the application, an evaluation of the coating tensile strength under cryogenic conditions was necessary. Hence, tubular coating tensile (TCT) tests were carried out at room temperature, cryogenic temperatures and after hydrogen charging. The details on the TCT specimens can be found in Figure 2 and the parameters in Table 1 aligning with (Hauer et al., 2023a; Hauer et al., 2024). A produced TCT test specimen consists of two coated round specimens, which are only connected on the outer surface by the thermally sprayed coating. The base materials or substrates for the TCT test pieces were designed in accordance with the standard EN 17393 (Technical Committee CEN/TC 240, 2020). All specimens were made of AISI 304 (1.4301) and had the dimensions Ø25 × 25 mm. The substrates for all other tests, i.e., flat substrates, were made of hot-rolled steel, also 1.4301, with dimensions of approx. 58 mm × 50 mm × 8 mm. Before spraying, all substrates were blasted with corundum and then cleaned with isopropyl alcohol. While the flat substrates were coated linearly, this movement was translated into a rotating movement for the TCT tests. For the latter, only *Arc Spray* was used (equipment as already described).

TABLE 1 Constant spray parameters of *Arc Spray*, see also (Hauer et al., 2023a).

Material	Voltage U in V	Current I in A	Wire feed rate v_{Wire} in m/min	Gas/p_{gas} in bar	Spray offset in mm	Robot speed in mm/s
Fe – partly amorphous	38	175	3.9	N2/6	5	500

DURMAT® AS-SNA-1090 wires with the composition FeCr28Ni7B3.5Mo1.5MnSi were used as filler materials, which corresponded to a combination of austenitic phases (~ AISI 316L) and amorphous phases (power source and wires from DURUM Verschleißschutz GmbH, Willich, DE; wires with d = 1.6 mm).

TABLE 2 Constant spray parameters of *HVOF Spray*, see also (Hauer et al., 2023b).

Parameter	Größe
Flow rate fuel gas (ethane) in L/min	110
Flow rate oxygen in L/min	170
Flow rate compressed air in L/min	360
Oxygen to fuel ratio	1.9–2.6
Powder feed rate in g/min	60
Stand-Off distance in mm	230
Robot speed in m/min	40

The powder GTV 80.44.1–0 (GTV Verschleißschutz GmbH, Luckenbach, DE; gas-atomized, fraction +45–15 µm), which is also a partially amorphous Fe alloy with the composition FeCr25B5C0.8, was used as an additive material.

2.2 Microstructure and chemical composition

For the microstructure analyses, the coated samples were first cut, cold-mounted in epoxy resin and then ground and polished step by step (until 3 µm diamond suspensions, finally oxide polish). A scanning electron microscope (SEM) JEOL JSM-IT100 (JEOL Germany GmbH, Freising, DE; acceleration voltage 10 kV, backscatter detector, high and low vacuum modes) and ImageJ software (National Institutes of Health, United States; using Despeckle filter, normalization and finally Trainable Weka Segmentation Tool) were used to examine the porosity/oxidation/crack content in the coatings at three locations in each sample. Representative analyses of morphology were also performed using the same equipment at different magnifications (×500, ×2,000).

In addition, energy dispersive X-ray spectrometry (EDS) was performed in the cross-sections at the same locations using a JEOL Dry SD25 detector (JEOL Germany GmbH, Freising, Germany; acceleration voltage 15 kV, high vacuum for metals and low vacuum for ceramics). In this way, the local chemical composition of the coatings was determined. EDS analyses were also carried out for the spray powders used for comparison purposes using the same equipment.

2.3 Thermal diffusivity

The thermal diffusivity was measured using an LFA 467 HT HyperFlash (Erich NETZSCH GmbH and Co. Holding KG, Selb, DE) on test specimens measuring 10 mm × 10 mm in the temperature range from 25°C to 300°C. As it was not possible to measure in a cryogenic environment, this range is as close as possible to low temperatures and provides a good impression of the insulation behavior. The gas used was Ar and the properties investigated, i.e., density, were of the stainless steel 1.4301. The test specimens were matted with graphite spray. The tests were carried out on all coating systems as well as on the pure base material.

2.4 Tubular coating tensile tests (TCT)

Quasi-static TCT tests were carried out in accordance with EN 17393 (Technical Committee CEN/TC 240, 2020) using a single-axis testing machine (Zwick Roell Z50, Ulm, DE). This test was carried out exclusively for the coatings *Arc Spray*. The temperature regimes used were room temperature and −110°C. In addition, a test series after cathodic hydrogen charging at room temperature was examined. The notch factor corresponded to 1.7 for all samples, while the microscopically determined coating thicknesses were used to calculate the coating cross-sectional area (Hauer et al., 2024). A cold gas system Isotherm TG-L63/100 (KGW-Isotherm Karlsruher Glastechnisches Werk—Schieder GmbH, Karlsruhe, Germany) with a vacuum-insulated stainless steel cryostat was used for the cryogenic experiments. Cathodic hydrogen charging was carried out using an aqueous solution with 3.5% NaCl as the electrolyte solution and a Pt anode. In addition, a laboratory power supply HMP 2020 (Rohde & Schwarz GmbH and Co. KG, Munich, DE) with a constant current density of 0.56 mA/cm³ and a voltage of 24 V was used. This led to a total hydrogen content of 7.70 ppm in the coatings after a charging time of approx. 91 h. The measurement of hydrogen was carried out by carrier gas hot extraction method using BRUKER G8 Galileo + IR-07 (Bruker Elemental GmbH, Kalkar, DE) at different desorption temperature regimes (Hauer et al., 2024). Figure 3 shows the generic test setup for the TCT tests using the example of testing under cryogenic conditions as well as the hydrogen charging procedure of the specimens.

Finally, only specimens that showed absolutely no misalignment at the transition between the coated specimens were used to determine the tensile strength. Additionally, some samples were used for preliminary tests, e.g., for determination of hydrogen

TABLE 3 Constant spray parameters of *Plasma Spray*.

Current in A	Flow rates Ar/H2 in L/min	Powder feed rate in g/min	Number of passes
380	20/10	12	30
		19	20
		25	12
420	25/10	12	26
		19	16
		25	10

Powders used corresponded to NiCrAlY Amperit 413.006 and YSZ Amperit 827.006 (both Höganäs Germany GmbH, Goslar, DE).

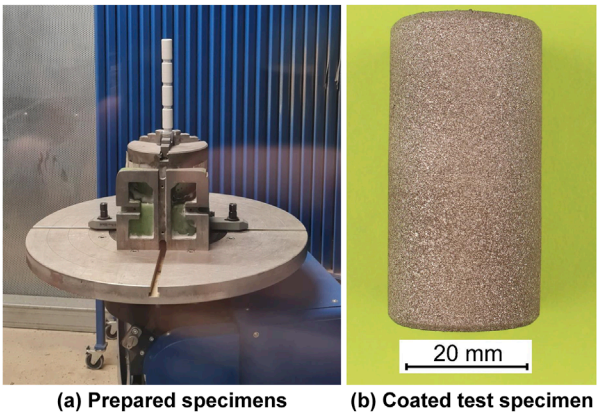

FIGURE 2
Coating process of TCT test specimens. Prepared specimens before spraying **(A)**, two specimens joined only by the coating as one TCT specimen **(B)**.

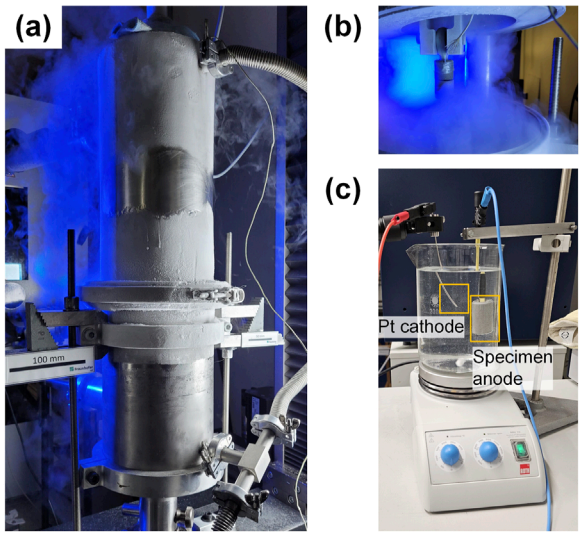

FIGURE 3
TCT Test setup under cryogenic conditions **(A)**. Specimen after fracture under cryogenic conditions **(B)**. The specimens were monitored using thermocouples. Experimental setup for hydrogen charging **(C)**.

charging parameters or the test setup and were thus not available for TCT testing. This means that ultimately the number of samples that could be evaluated at room temperature was 18 while the number of samples that could be analyzed at cryogenic temperature was 15. For the test series after hydrogen charging, 9 samples could be used.

2.5 Production of a pipe demonstrator

Th new dual tank concept is shown in Figure 4. First, it is based on the production of a hybrid pipe demonstrator. The best performing variants from the previous tests from both concept parts were used for this. These were chosen together with the partners involved in the study.

For thermal spraying, this corresponds to arc wire spraying with the above-mentioned filler material. However, a Sparc 400 power source and a Shark RE torch (by GTV Verschleißschutz GmbH, Luckenbach, DE) were used for production, while the spray parameters were identical, see Table 1. In order to realize the advantageous coating properties, the linear kinematics had to be converted into a rotating movement, which corresponded in principle to the previous tests. This was implemented via the constancy of the relative movement.

A laboratory winding system, which basically consists of two controlled axes (rotatory and translatory), a braked roving supply spool, an impregnation bath with resin stripper and a thread eye for depositing, was used to produce the FRP winding from glass fiber reinforced plastic (GRP). The radially wound FRP steel pipe samples were manufactured using the wet winding process. The pipe to be wound with an outer diameter of 60 mm was itself used as the winding mandrel. The pipe is supported and tensioned on a threaded rod using two cones. An E-CR glass fiber direct roving D906 (roving fineness 2,400 tex, roving width 5 mm) was used as fiber reinforcement. This has a soft silane coating, which is particularly recommended for wrapping and is compatible with thermosetting

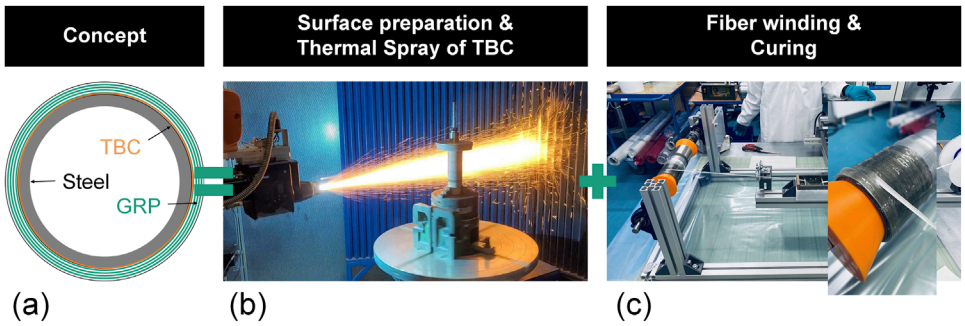

FIGURE 4
Novel tank concept: dual concept for LH_2 tanks. Schematic drawing **(A)**, subsequent surface roughening and thermal spraying of a TBC **(B)** and final fiber winding and curing **(C)** based on the example of a pipe demonstrator.

resin systems. The resin system used was the toughened 3-component epoxy resin system Biresin® CR141 from Sika Germany. Due to its low viscosity, good wetting properties and very long pot life, the resin system is suitable for wet winding. The choice of GRP as the material for the winding is based on its low thermal conductivity and low material costs in addition to its excellent specific strength and rigidity. Another special requirement for the hybrid FRP-steel tank concept is the high temperature range. LH_2 tanks are heated to 100°C during evacuation and cooled down to −253°C during operation. As a result, the hybrid tank concept experiences high temperature-induced distortions. The similar coefficients of thermal expansion of GRP in the fiber direction and steel help to minimize temperature-induced residual stresses in the materials. For radial winding of the pipe demonstrator, a rotational speed of the rotation axis of 5 revolutions/min and a translational feed rate of 25 mm/min were selected as the winding parameters. The thread tension of the roving was measured and monitored during the winding process using a thread tension sensor. After depositing the impregnated glass fiber rovings, a perforated shrink tape (type HI-Shrink Tape from Dunstone) was applied for curing. This shrinks by up to 20% during curing in the oven and thus compresses the winding. This also results in a smoother surface of the pipe samples. The curing of the GRP winding takes place according to the manufacturer's instructions at two temperature levels for 3 h at 80°C and then a further 3 h at 120°C.

Finally, the pipe demonstrator was visually inspected and documented macroscopically and photographically. The final thicknesses of the various stages were determined using calibrated calipers.

2.6 Production and testing of a tank demonstrator

The production and testing of the pipe demonstrator formed the basis for the complete coating, fiber winding and subsequent testing of a small hybrid prototype tank. The different procedures and methods shall be quickly summarized in the following. After the cryogenic and compression set tests, the hybrid tank was visually inspected to identify possible changes.

2.6.1 Production

The basis for the technology demonstrator and reference for comparison is a simple compressed air storage tank of the type CRVZS-10 from Festo with a volume of 10 L and an operating pressure of −0.95–16 bar. The geometric dimensions are as follows: Length: 558 mm, diameter: 160 mm, wall thickness: 2.5 mm. In the first step, the two base frames and the condensate drain were removed from the cylindrical area of the tank using an angle grinder and then the open hole from the condensate drain was welded up and ground flat. In the next steps, the thermal spraying of the TBC and the fiber winding process could be carried out in the cylindrical area of the tank in the same way as the production of the pipe demonstrator.

To reduce the winding time, the rotational speed of the rotational axis was varied between 5–20 revolutions/min and the translational feed rate was varied accordingly between 25–100 mm/min, in contrast to the previous production test. A total of 5 radial windings were applied in the cylindrical area. Furthermore, a fiber-optic strain sensor with an imprinted fiber Bragg grating (FBG) was inserted between the 3rd and 4th fiber layer in the circumferential direction (fiber direction). For recording the strains, a measuring amplifier (interrogator FBG-Scan 908 from FBGS Technologies GmbH) was used. The curing of the winded demonstrator tank in the temper oven, including instrumentation, is shown in Figure 5.

2.6.2 Cryogenic tests

After production, the winded hybrid tank was subjected to a low-temperature test. For this purpose, it was filled with dry ice in a vertical position in an insulation box and checked for possible temperature changes (thermal insulation properties). For comparison purposes, an identical tank was tested in parallel in the same way as a reference without the new tank concept. The mass of the dry ice introduced was weighed using a scale and was found to be identical for both tanks. The test setup is shown in Figure 6.

2.6.3 Compression set tests

Following the low-temperature test, the hybrid tank was cyclically filled with compressed air up to 8 bar several times and the corresponding longitudinal deformation at the end of the dome and the radial deformation in the cylindrical area were recorded using a calibrated, digital dial gauge (MarCator 1075R

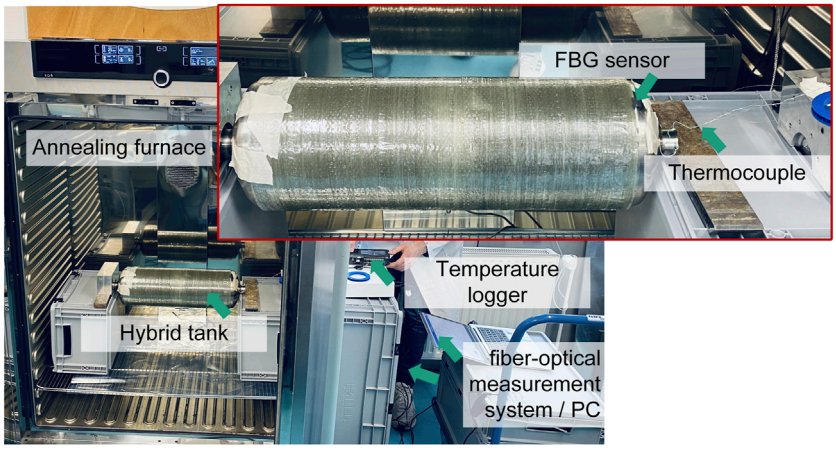

FIGURE 5
Instrumentation and measurement setup of the wound tank demonstrator during curing.

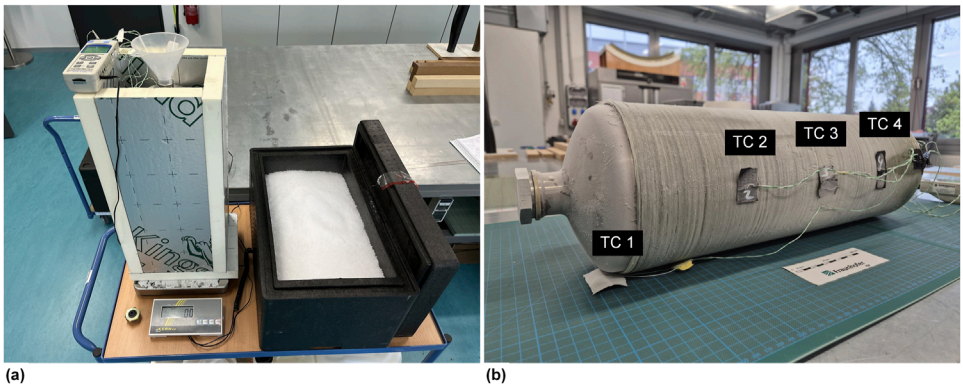

FIGURE 6
Test setup for dry ice filling including external insulation **(A)** and measuring points of thermocouples 1 to 4 **(B)** for coated and wound hybrid tank (after completion of measurement). The same procedure was used for the reference tank.

from Mahr, measuring accuracy 1 µm). The internal pressure was measured using a digital pressure gauge from PCE-Instruments. For comparison, the deformation measurement was also carried out on the reference tank without TBC layer and GRP winding. The tank was firmly clamped in a machine vice at one end of the dome and simply supported on the other end of the dome so that corresponding displacements were tolerated. The test setup is shown in Figure 7.

3 Results

3.1 Coating morphology and composition

Figure 8 shows the typical microstructures and chemical compositions of the various coating systems investigated.

First of all, it should be noted that the coatings have completely different morphologies, despite the similarities of the materials, e.g., for *Arc Spray* and *HVOF Spray*. In addition, these two coatings show very good adhesion to the substrate, whereas for *Plasma Spray* some detachment occurred during the microsection preparation. In terms of defect content, the *HVOF Spray* coatings exhibit the lowest values, whereas *Arc Spray* and *Plasma Spray* are comparable when standard deviation is considered. However, all coatings have comparatively low defect contents of less than 5%, with these being dominated by porosity.

The *HVOF Spray* coatings show very little oxide formation near the particle interfaces. The morphology can be described as irregular and spherical with partially containing insufficiently molten particles. Different phases are visible through the material contrast. These include lighter and darker gray areas with an initial powder structure, as well as bright white irregular particles. The latter are clearly distinguishable from the surrounding coating. Regarding the composition, it should be noted that the overlapping of the peaks of the light elements B and C as well as the rather low B content complicate the analysis. However, in combination with other analyses, it was found that P2 corresponds to a mixture of hard phases with B, C and Cr (carbides, carborides) and the typical alloy composition with some burn-off losses. The original

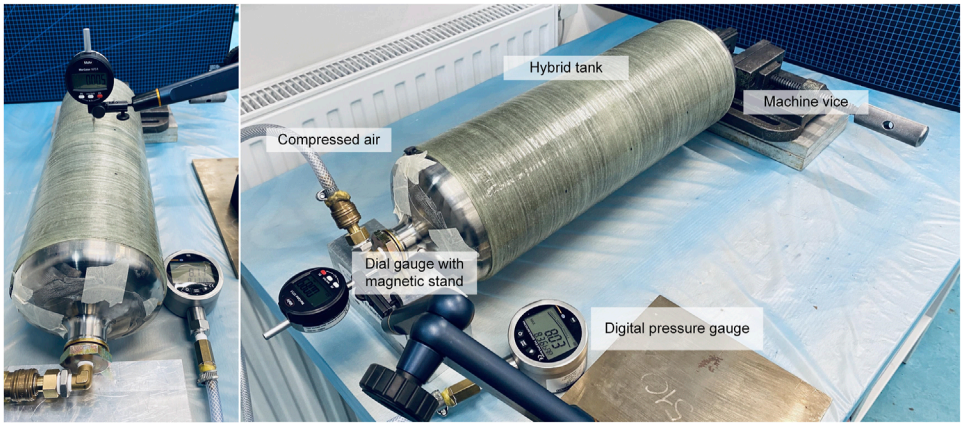

FIGURE 7
Test setup for compression deformation test with hybrid tank for measuring radial (left) and longitudinal deformations (right).

powder structure was largely retained, which is consistent in the SEM images. Nevertheless, there are differences to P1, which also contains Mo. Finally, particles based on WC-CoCr were detected in P3, which were not part of the original powder.

The *Arc Spray* coatings have a lamellar structure typical for the spraying process, even if the size of the lamellae varies considerably in some cases. Both amorphous and classic crystalline-dendritic solidified areas occur about equally, which can be easily recognized by the contrast. Irregularly shaped oxides and accumulated porosity are also visible. Some hard phases could be identified in the material, which is confirmed by the chemical analyses. Point P4 is in the crystalline region of the material, which is reflected by the composition, which essentially corresponds to a highly alloyed stainless steel. P5, on the other hand, has a more amorphous composition. P6, on the other hand, corresponds to a hard phase of B, C and Cr (carborides). The bundled porosity of P7 contains oxygen-affine elements such as Al together with O itself.

The coatings *Plasma Spray* show an irregular morphology with some insufficiently molten particles, which leads to accumulated porosity in some cases. Regarding the material contrast, there are apparently no recognizable differences between the various phases. The observations are confirmed in the EDS investigations, which show hardly any differences to each other. The absence of Y compared to the powder and traces of Cu and Ca are also noticeable. In addition, some particles are clearly separated from the coating.

3.2 Thermal insulation behavior

In Figure 9, the thermal diffusivities of the coatings are compared with the uncoated substrate, i.e., tank material. First, it can be seen that all materials and processes have significantly lower values compared to the substrate, with the lowest values overall for *Plasma Spray*. In addition, a slight curvature of the graph at lower temperatures can be seen for the substrate, which was not observed for the coatings.

The diffusivity of the substrate is above that of *HVOF Spray* with a factor of around 1.6. Similar orders of magnitude are found when comparing *HVOF Spray* with *Arc Spray*. The *Arc Spray* coatings therefore exhibit a lower diffusivity by a factor of 2.3 on average compared to the uncoated substrate. The overall slope of the curve also appears to be lower than for *HVOF Spray* and the substrate material. The lowest values and therefore the highest insulation capabilities are found in the measurements for *Plasma Spray*, with slightly higher values at the lowest temperatures.

3.3 Coating tensile strength

In Figure 10, the coating tensile strengths after different test regimes are shown for *Arc Spray*.

Firstly, an increase in the tensile strength of the coating from RT to −110°C of around 30% can be observed. Nevertheless, the standard deviation for cryogenic temperatures is higher than for RT. However, a comparison with the samples charged with hydrogen shows a small decrease of roughly 7% compared to the samples at RT. The scattering of the charged specimens is the overall smallest of all the data presented. Yet, in this case, the different batch sizes must be taken into account.

3.4 Pipe demonstrator results

The results of the production of the pipe demonstrator are shown in Figure 11. The two concept parts were successfully combined, i.e., the fiber winding could be applied to the thermally sprayed coating without any process-related problems.

The thicknesses of the various stages are within the expected range with a coating thickness of around 200 µm for the TBC and 2.3 mm for the fiber winding.

3.5 Tank demonstrator results

3.5.1 Curing process

The temperature and the strains (radial) in the GRP winding were measured, see Figure 12.

10.3389/fenrg.2024.1441746

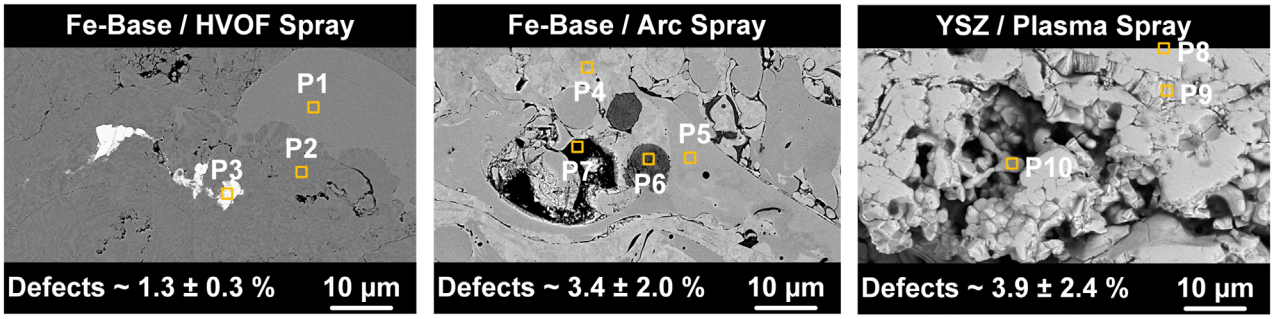

Composition in Wt%	B	C	O	Si	Cr	Mn	Fe	Co	Mo	W
Fe-Base / HVOF Spray										
P1	n.d.	5.54	n.d.	0.95	26.12	n.d.	50.70	n.d.	3.88	n.d.
P2	n.d.	6.75	n.d.	0.19	28.04	n.d.	64.98	n.d.	n.d.	n.d.
P3	n.d.	5.12	n.d.	0.27	8.17	n.d.	22.42	3.64	n.d.	60.37
Fe-Base / Powder	*1.3 ± 0.6*	*5.2 ± 0.1*	*n.d.*	*0.3 ± 0.0*	*25.3 ± 0.1*	*n.d.*	*68.0 ± 0.4*	*n.d.*	*n.d.*	*n.d.*

Composition in Wt%	B	C	O	Si	Cr	Mn	Fe	Ni	Mo
Fe-Base / Arc Spray									
P4	n.d.	3.16	0.30	0.77	18.83	1.70	60.54	11.81	2.89
P5	0.10	2.81	n.d.	0.33	38.60	0.48	56.46	0.86	0.36
P6	12.97	4.09	n.d.	0.16	51.85	0.49	29.70	0.71	0.04
P7	n.d.	10.58	13.71	1.13	18.20	0.78	50.31	4.14	0.46
*Fe-Base / Wire**	*< 5.0*	*< 0.1*	-	*< 1.0*	*28*	*< 1.0*	*Bal.*	*7*	*1.5*

Composition in Wt%	C	O	Mg	Al	Ca	Cu	Y	Zr	Hf
YSZ / Plasma Spray									
P8	28.56	25.64	n.d.	n.d.	0.39	0.35	n.d.	45.06	n.d.
P9	27.36	26.75	n.d.	n.d.	0.35	0.33	n.d.	45.22	n.d.
P10	26.84	29.71	n.d.	n.d.	0.29	0.43	n.d.	42.73	n.d.
YSZ / Powder	*10.1 ± 0.2*	*29.9 ± 0.9*	*n.d.*	*0.1 ± 0.0*	*n.d.*	*n.d.*	*5.5 ± 0.1*	*53.4 ± 1.0*	*1.0 ± 0.1*

FIGURE 8
Morphology and defect content (sum of porosity, oxidation, cracks) of the various thermally sprayed coatings (top) and chemical composition at selected points/phase components (bottom).*Only nominal values of the manufacturer are available for the wire, no own analyses. "n.d." stands for not detectable.

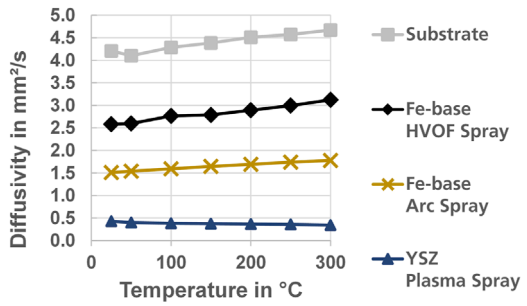

FIGURE 9
Thermal diffusivity of the thermally sprayed coatings in relation to the substrate, i.e., tank material.

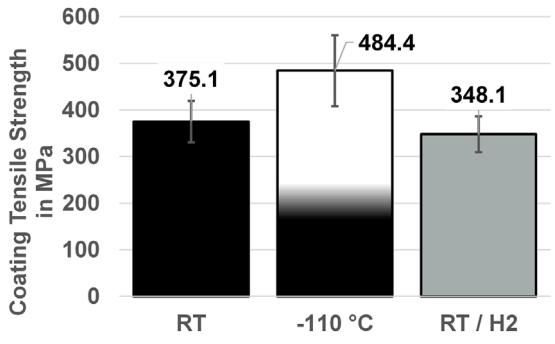

FIGURE 10
Coating tensile strength for various test regimes at RT, −110°C as well as RT and after hydrogen charging.

By using the fiber optic measuring system, valid thermally induced distortions could be determined. The measurement curves show a maximum strain of approx. 580 µm/m (black curve) when the oven temperature of 70°C is reached. Due to the curing reaction of the epoxy resin used and the resulting exotherm, there is an increase in temperature in the GRP winding, which was not measured directly here, resulting in a strain peak. During the further tempering process, the strain remains at a constant level of approx. 400 µm/m, while it drops to a negative value of approx. −440 µm/m

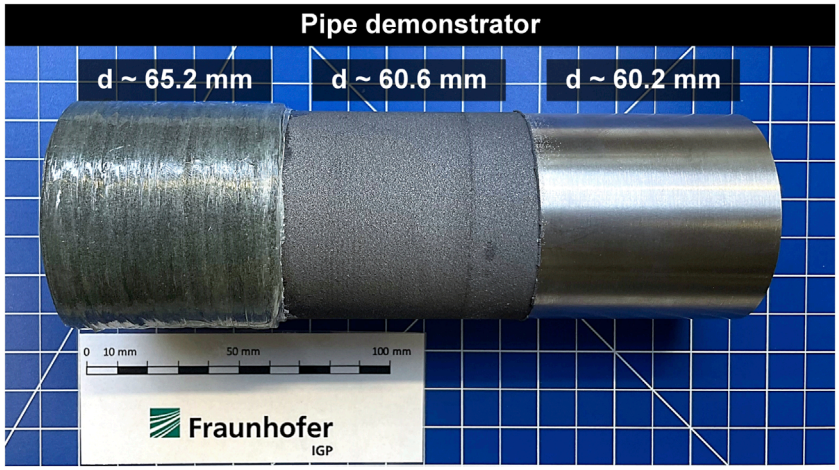

FIGURE 11
Finished pipe demonstrator and coating thicknesses measured using a caliper gauge.

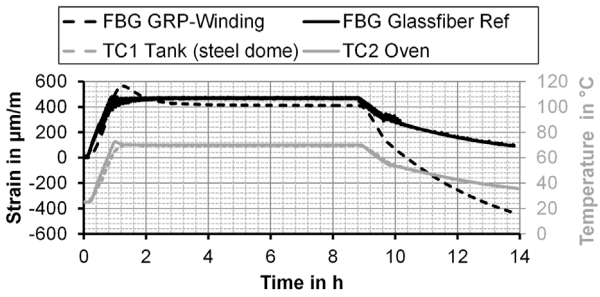

FIGURE 12
Strain and temperature measurement data during the curing process.

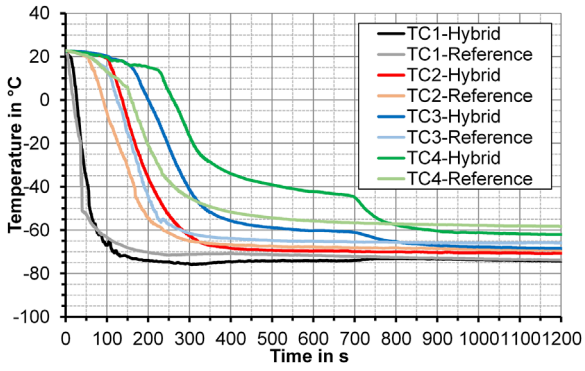

FIGURE 13
Temperature curves of hybrid and reference tank for the various thermocouples.

at a temperature of 35°C during cooling. In contrast, the reference FBG sensor, which is unloaded in the temper oven, almost returns to its initial value, considering the oven temperature. The measurement data thus show that during the curing process of the GRP winding, corresponding thermal distortions are frozen and lead to residual stresses in the hybrid tank. The steel tank expands during the heating process, while the uncured resin of the GRP winding is still flexible. After gelling, cross-linking occurs and the resin and thus the composite harden, with a corresponding time delay. During the cooling process, the steel tank shrinks more than the GRP winding due to different thermal expansion coefficients and ultimately leads to thermally induced residual compressive stresses in the fiber composite winding, which are recognizable in the negative strains.

3.5.2 Cryogenic behavior

The results of the temperature measurements during and after dry ice exposure are shown in Figure 13.

In general, all curves have in common that, regardless of the concept used, the differences disappear with longer measurement duration, so that the curves are almost congruent. Furthermore, it is obvious that the characteristics of the curves are highly dependent on the point of measurement. The largest average differences are evident at TC4 (highest measuring point), the smallest at TC1 (lowest measuring point), particularly in the range up to around 500 s. These trends become even more apparent when comparing the time taken to reach specific temperatures, see Table 4. In the cylindrical part of the tank with GRP winding and thermally sprayed coating, time differences can be clearly seen at measuring points TC2 to TC4.

3.5.3 Compression set behavior

The measured longitudinal and radial deformations from the pressure test for the two tanks examined are compared in Table 5.

With regard to the longitudinal deformations, both tanks show a similar result. At a pressure of 8 bar, the tanks expand by approx. 0.088 and 0.086 mm respectively. It can be seen that the GRP winding, which is only applied in the cylindrical area, has no influence on the longitudinal deformation. However, clear differences can be observed in the radial deformations. At an internal pressure of 8 bar, the reference tank deforms in a negative direction

TABLE 4 Times to reach −20°C, −40°C, and −55°C at the various measuring points (TC1-TC4) for hybrid and reference tank in comparison as well as the resulting delta.

	TC1			TC2			TC3			TC4		
T in °C	Hybrid in s	Ref in s	**Delta in s**	Hybrid in s	Ref in s	**Delta in s**	Hybrid in s	Ref in s	**Delta in s**	Hybrid in s	Ref in s	**Delta in s**
−20	38	37	**1**	169	127	**42**	247	159	**88**	309	198	**111**
−40	55	40	**15**	212	166	**46**	297	191	**106**	521	264	**257**
−55	65	57	**8**	260	204	**56**	388	227	**161**	759	536	**223**

TABLE 5 Comparison of measured longitudinal and radial deformations from compression set test for hybrid and reference tank and resulting delta.

	Pressure in bar	Hybrid-tank	Reference-tank	Delta
Longitudinal deformation in mm	4	0.045	0.042	**0.003**
	8	0.088	0.086	**0.002**
Radial deformation in mm	8	0.006	−0.016	**0.022**

by −0.016 mm, i.e., it is tapered in the cylindrical area. The hybrid tank with the GRP circumferential windings shows its increased rigidity here and does not taper radially, but expands by a minimum of 0.006 mm. After the low-temperature and compression set tests, the hybrid tank was visually inspected in detail. On a macroscopic level, no optical changes, such as white fractures in the GRP winding due to inter-fiber fractures, were visible.

4 Discussion

In the first part, the coating properties achieved will be considered and classified regarding the application and demanding specifications. In the second part, the implemented dual manufacturing concept and resulting hybrid prototypes will be evaluated.

4.1 Insights into coating properties and evaluation

The microstructural analyses initially revealed that the thermally sprayed coatings exhibit completely different morphologies despite their partially similar chemical composition, although the properties, for example, regarding the defect content, are comparable and can be classified as favorable.

The *HVOF Spray* coatings showed a comparatively high defect content for this process, which was primarily dominated by porosity. This is mainly due to the non-ideal parameter set and therefore sub-optimal coating structure for the new powder, which can also be seen in the partially unmolten particles. The relatively slow traverse speed of the kinematics also plays a role here—however, faster speeds would have led to even worse heating of the powder. This, in turn, would have resulted in a further reduction in deposition and coating build-up. In addition, individual, bright white particle clusters in the micro-sections could be attributed to WC-CoCr contamination due to previous spray experiments, which may have caused an interaction with the rest of the coating. The thermal diffusivity nevertheless showed promising results for *HVOF Spray*, albeit worse than for the other spray processes. An optimization of the powder in the sense of a finer fraction and thus also more finely distributed porosity would therefore be appropriate to achieve more uniform heating in the particle-free jet. This would allow the use of the full potential of the HVOF technology for the application.

For *Arc Spray*, a low defect content could be determined for the process, which was also dominated by porosity. Due to the special mixing of the crystalline, amorphous, and hard phases, however, accumulated pore formation took place at the interfaces, but did not seem to interfere with the crucial coating properties. On the other hand, the usual oxidation could be completely suppressed by using nitrogen as the atomizing gas. These observations show that the structure of the coatings with the opposing mechanisms of nucleation and amorphous phase formation depends very strongly on the parameters used as well as the composition of the alloys. Moreover, the investigations of the thermal diffusivity showed the best results for all metallic coatings during the study, although being comparably higher than for the *Plasma Spray* coatings. This is presumably due to the internal material transitions between amorphous and crystalline phases and the associated inertia of the heat transfer. On the other hand, other advantageous properties such as cryogenic durability and high mechanical properties such as hardness were observed in (Hauer et al., 2023a).

As expected, the ceramic coatings *Plasma Spray* showed the best properties in terms of thermal diffusivity. The correlation to porosity was also visible here, i.e., a higher porosity for ceramic materials is generally beneficial to achieve low diffusivity values (Vassen et al., 2009). At the same time, the higher porosity is not a main factor in terms of delamination since it is caused

mainly by residual stresses and less adhesion to the substrate (Liu et al., 2019; Chi et al., 2014; Hauer et al., 2017). Nevertheless, these ceramic coatings proved to be unsuitable for cryogenic temperatures, which cause delamination by enhancing the intrinsic stresses and overcoming adhesion.

The combination of properties mentioned above led to the selection of *Arc Spray* coatings for the coating tensile tests and demonstrator production, as this process represents the best compromise of coating properties [see (Hauer et al., 2023a; Hauer et al., 2023b; Hauer et al., 2024)] and can also be used economically on a large scale. In terms of tensile strength, it could be shown that cryogenic temperatures during testing lead to a severe increase, while the accumulation of hydrogen results in only a small decrease in strength. Both effects are generally beneficial for the application, while the exact mechanisms are still unclear and remain to be investigated further. The difference in coating formation between the austenitic and the amorphous phases in this material could contribute to possibly only allowing local coating changes. It has also been shown that spraying with nitrogen can reduce the residual stresses in coatings compared to spraying with compressed air. This could also have a positive effect on tensile stresses present in the material. As for the influence of hydrogen, the usual concepts, e.g., for enrichment at the crack tip, are plausible but still need to be substantiated by further investigations.

4.2 Key factors of the dual concept and assessment of resulting hybrid prototypes

It was shown that a combination of the two technologies is possible and easy to implement in terms of production technology as a dual concept. As a result, both, the TBC coatings, and the fiber windings could be applied consecutively in sufficient thickness and in a defined manner. These successful investigations on the hybrid pipe demonstrator formed the basis for the complete coating and fiber winding of a small hybrid tank demonstrator, which was compared to reference design in certain aspects. These aspects of the dual concept shall be discussed in the following.

In general, a significant and positive effect of the hybrid tank concept on the insulation capability can be determined. In the cylindrical part of the tank with GRP winding and the underlying thermally sprayed coating, substantial time differences between the concepts can be seen, e.g., at the measuring points TC2 to TC4, supporting this thesis. The rather small temperature differences at TC1 are due to the fact that it is positioned in the lower dome area, where both, the reference tank and the hybrid tank are only consisting of steel and where the tank also first comes into contact with dry ice. Process-related measurement errors in the filling tests result to a large extent from the filling speed, which was not identical in both tests due to the manual filling. Another factor that should not be neglected is the slight difference in the location of the measuring points themselves. Due to the prototypical coating, the hybrid tank also has uncoated ends, which, together with the factors mentioned above, cause deviations in the temperature gradient and course from the overall trends.

Furthermore, in terms of compression set, the hybrid tank with the GRP circumferential windings showed an increased rigidity. It expanded radially, in contrast to the reference design. Still, it should be noted that due to the undulations of the GRP surface, tactile measurement in the radial direction is rather prone to error. An alternative would be an optical measurement with a high-precision 3D measuring system, e.g., using a stripe light projector or digital image correlation using GOM Aramis. However, the tendency towards different deformation behavior of the two tank concepts is clearly evident. After the cryogenic and compression set test, the hybrid tank was visually inspected and did not show any changes on a macroscopic level indicating stability of the applied structures.

In conclusion, it was found that the developed dual concept could successfully be implemented not only on a pipe, but also on a small tank. Measurable differences compared to the reference tank design could be observed.

5 Summary and outlook

As part of a research on LH_2 tanks, two innovative technical concepts from aerospace and high-temperature applications were successfully adopted, combined, and qualified for use in the wind-power-to-gas scenario. The focus was on the requirements for transport weight, strength, insulation, and cryogenic durability. New material concepts were successfully established, particularly in the area of TBC. They exhibited an outstanding combination of thermal insulation and high mechanical characteristics in low temperature as well as high resistance to hydrogen in the form of only slightly modified properties. These successful tests formed the basis for the complete coating, fiber winding and subsequent testing of a small hybrid tank. This tank demonstrator showed promising properties regarding insulation in cryogenic environments and an improvement in deformation behavior, when compared to the reference design. Thus, the dual concept presented in this work could lay the foundation for a scalable concept for future use in large structures such as LH_2 tanks and pipelines or for alternative fuels in the maritime sector. In terms of costs, it is not possible to make a final statement yet at the present time, because tank concepts and costs vary considerably. It is certain that the manufacturing costs will be higher initially, but amortization will occur over time due to the reduced weight (fuel and material savings) and the improved LH_2 efficiency (lower boil-off, less maintenance due to better properties).

Data availability statement

The raw data supporting the conclusions of this article will be made available by the authors, without undue reservation upon reasonable request.

Author contributions

MH: Data curation, Funding acquisition, Investigation, Methodology, Supervision, Validation, Writing–original draft, Writing–review and editing. SS: Data curation, Funding acquisition, Investigation, Methodology, Project administration, Supervision, Validation, Writing–original draft, Writing–review and editing. AG: Conceptualization, Project administration, Supervision,

Visualization, Writing–original draft, Writing–review and editing. OB: Data curation, Investigation, Methodology, Validation, Visualization, Writing–original draft, Writing–review and editing. LM: Data curation, Investigation, Methodology, Validation, Visualization, Writing–original draft, Writing–review and editing. PB: Data curation, Investigation, Methodology, Validation, Visualization, Writing–original draft, Writing–review and editing. NS: Data curation, Investigation, Methodology, Validation, Visualization, Writing–original draft, Writing–review and editing. K-MH: Conceptualization, Funding acquisition, Supervision, Writing–original draft, Writing–review and editing.

Funding

The author(s) declare that financial support was received for the research, authorship, and/or publication of this article. The research project IGF 39 LBR 1/Increasing the storage and transport efficiency for liquid hydrogen in steel fiber composite tanks by thermally sprayed TBC coatings (LH2 tanks) from the Research Association for steel Application (FOSTA), Düsseldorf, is supported by the Federal Ministry of Economic Affairs and Climate Action, the German Federation of Industrial Research Associations (AiF) as part of the programme for promoting industrial cooperative research (IGF) on the basis of a decision by the German Bundestag. The project is carried out at Fraunhofer IGP in the framework of the overall project entitled Offshore Wind Energy Systems for Hydrogen Supply. We thank for the funding, the cooperation with other research institutes and for the input by the participating companies.

Acknowledgments

The authors would like to thank all co-workers involved in the study, namely, listed in alphabetical order: B. Allebrodt, P. Andreazza, M. Brandes, J. Broer, J. Hilbert, F. Knöchelmann, W. Krömmer, V. Nikolova, N. Peters, A. Piecha, M. Reich, L. Sattler, S. Schneider, M. Schur, L. Steinmetz and N. Ziegelmann.

Conflict of interest

The authors declare that the research was conducted in the absence of any commercial or financial relationships that could be construed as a potential conflict of interest.

Publisher's note

References

Bach, F.-W., Möhwald, K., Laarmann, A., and Wenz, T. (2005). "Modern coating processes," in *German: moderne beschichtungsverfahren* (Weinheim: Wiley VCH).

Chi, J., Zhang, A., Xie, S., and Jin, C. (2014). Process optimization and residual stress measurement for Arc spraying rapid tooling. *J. Xi'an Jiaot. Univ.* 48 (12), 126–130.

Degenhardt, R. (2016). "Load-bearing structures made of fiber composites - new subject area of the Lower Saxony Chamber of Engineers," in *Ger. Tragkonstruktionen aus Faserverbunden – neues Sachgeb. Ingenieurkammer Niedersachs. CFK Valley. Innov. Rep. 1*, 201.

Dobler, K., Kreye, H., and Schwetzke, R. (2000). Oxidation of stainless steel in the high velocity oxy-fuel process. *J. Therm. Spray. Technol.* 9 (3), 407–413. doi:10.1361/105996300770349872

European Commission (2020). "A European green deal. Brussels," in *German: europäische kommission (2020):ein europäischer green deal. Brüssel.* Available at: https://ec.europa.eu/info/strategy/priorities-2019-2024/european-green-deal_de (Accessed May 31, 2024).

Fraunhofer, I. S. I., and Fraunhofer, I. S. E. (2024). "A hydrogen roadmap for Germany. Freiburg," *German: Eine Wasserstoff-Roadmap für Deutschland. Freiburg*. Available at: https://www.ise.fraunhofer.de/content/dam/ise/de/documents/publications/studies/2019-10_Fraunhofer_Wasserstoff-Roadmap_fuer_Deutschland.pdf (Accessed May 31, 2024).

Frost, Sullivan, (2020). *Study on disruptive innovations in production, storage, and transportation of hydrogen* (Santa Clara US-CA).

German, B. M. (2020). "Wi: The national hydrogen strategy. Federal Ministry for Economic Affairs and Energy," in *German: Die Nationale Wasserstoffstrategie. Bundesministerium für Wirtschaft und Energie (Hrsg.)* (Status).

Hauer, M., Gericke, A., Möhrke, L., Allebrodt, B., and Henkel, K.-M. (2023a). Highly efficient thermal barrier coatings based on arc spraying of amorphous Fe-based alloys and NiCrAlY for use in LH2 tanks and other cryogenic environments. *J. Therm. Spray Technol.* 32 (2), 327–338. doi:10.1007/s11666-023-01548-8

Hauer, M., Gericke, A., Möhrke, L., Krömmer, W., and Henkel, K.-M. (2023b). "Novel Fe- and Ni-based HVOF-sprayed coatings for improved thermal insulation in cryogenic environments," in Proceedings of the International Thermal Spray Conference and Exposition, Mai, Québec City, Canada. Editor F. Azarmi (ASM International), 357–364. doi:10.31399/asm.cp.itsc2023p0357

Hauer, M., Henkel, K. M., Krebs, S., and Kroemmer, W. (2017). Study of traverse speed effects on residual stress state and cavitation erosion behavior of Arc-sprayed aluminum bronze coatings. *J. Therm. Spray. Tech.* 26 (1-2), 217–228. doi:10.1007/s11666-016-0446-0

Hauer, M., Möhrke, L., Biswal, P., Brätz, O., Gericke, A., Allebrodt, B., et al. (2024). "Properties of Novel partially amorphous Fe-based thermal barrier coatings under the influence of cryogenic temperature and hydrogen," in Proceedings of the International Thermal Spray Conference and Exposition, Mai, Milan, Italy, April – 01.29, 2024, 204–212. DVS Reports, Issue 393, DVS Media 2024. doi:10.31399/asm.cp.itsc2024p0204

Holloman, L., and Levy, A. V. (1992). Ceramic-coated components for the combustion zone of natural gas engines. *J. Therm. Spray. Tech.* 1 (1), 27–31. doi:10.1007/bf02657014

Kim, J.-H., and Lee, M.-H. (2010). A study on cavitation erosion and corrosion behavior of Al-Zn-Cu-and Fe-based coatings prepared by arc spraying. *J. Therm. Spray. Tech.* 19 (6), 1224–1230. doi:10.1007/s11666-010-9521-0

Kreye, H., Gärtner, F., Kirsten, A., and Schwetzke, R. (2000). "High velocity oxy-fuel flame spray: state of the art, prospects and alternatives," in *Proc. HVOF spraying: november 16-17, 2000, erding, Germany*. Editor P. Heinrich (Gemeinschaft Thermisches Spritzen e.V.), 5–16.

Krömmer, W., and Heinrich, P. (2009). "Influence of gases in thermal spraying," in *Proc. Hvof Spraying: november 5-6, 2009, Erding, Germany; focal point: cold spraying, equipment, applications*. Editor C. Penszior (Gemeinschaft Thermisches Spritzen e.V), 117–121.

Lang, F., and Krömmer, W. (2015). "Economic and ecological benefits of using gas mixtures for Arc spraying, tagungsunterlagen 10 kolloquium hochgeschwindigkeits-flammspritzen/10Th colloquium hvof spraying: 29. Und 30," in Oktober 2015, Erding, Conference Proceedings. Editor C. Penszior (Gemeinschaft Thermisches Spritzen e.V), 79–88.

Lima, R. S., Guerreiro, B. M. H., and Marple, B. R. (2017). "Comparing the microstructures and properties of YSZ TBCS manufactured via air plasma spray (APS), suspension plasma spray (SPS) and finely-dispersed-particle air plasma spray (FAPS)," in ITSC 2017 - International Thermal Spray Conference and Exposition: Abstracts of the Conference in Düsseldorf (DVS Media GmbH), 388–393.

Lima, R. S., Guerreiro, M. H., Curry, N., Leitner, M., and Körner, K. (2019). "Environmental, economical and performance impacts of Ar/H2 and N2/H2 plasma sprayed YSZ TBCS," in ITSC 2019: International thermal spray conference and exposition 2019 conference proceedings. Editor F. Azarmi (ASM International), 71–78.

Liu, Z., Feng, Y., Lei, G., and Li, Y. (2019). Fluid sloshing dynamic performance in a liquid hydrogen tank. *Int. J. Hydrogen Energy* 44 (26), 13885–13894. doi:10.1016/j.ijhydene.2019.04.014

Mathesius, H.-A., and Krömmer, W. (2014). *Practice of thermal spraying Guidance for technical personnel*, 2. DVS Media.

Pawłowski, L. (2008). *The science and engineering of thermal spray coatings*, 2. Wiley. doi:10.1002/9780470754085

Pinto, H., Pyzalla, A., Büscher, R., Fischer, A., Aßmus, K., and Hübner, W. (2005). The effect of hydrogen on the deterioration of austenitic steels during wear at cryogenic temperature. *Wear* 259 (1-6), 424–431. doi:10.1016/j.wear.2005.02.057

Technical Committee CEN/TC 240 (2020). *Thermal spraying and thermally sprayed coatings, Thermal Spraying – tubular coating tensile test, EN 17393*. Brussels: CENELEC.

Terberger, P. (2015). "Aging of vacuum plasma sprayed MCrAlY protective coatings and their interaction with nickel- and cobalt-based γ/γ'-superalloys. Doctoral thesis. Research Center Jülich GmbH," in *German: Alterung von Vakuum-Plasmagespritzten MCrAlY-Schutzschichten Und ihre Wechselwirkung mit Nickel-und Cobalt-basierten γ/γ'-Superlegierungen. Dissertation. Forschungszentrum Jülich GmbH*.

Vassen, R., Stuke, A., and Stöver, D. (2009). Recent developments in the field of thermal barrier coatings. *J. Therm. Spray. Tech.* 18 (2), 181–186. doi:10.1007/s11666-009-9312-7

Wielage, B., Wank, A., Pokhmurska, H., Grund, T., Rupprecht, C., Reisel, G., et al. (2006). Development and trends in HVOF spraying technology. *Surf. Coat. Technol.* 201 (5), 2032–2037. doi:10.1016/j.surfcoat.2006.04.049